Effect of Ash and Sulphate on Corrosion of Ni-Based Alloys in a Simulated Oxyfuel Combustion Environment

Xuteng Xi[1] · Jianqiang Zhang[1] · David J. Young[1]

Abstract

Alloys of Ni–25Cr–(2Mn–1Si) under mixed deposits of ash + (0, 10, 50 and 90) wt% sulphate were exposed to an Ar–$60CO_2$–$20H_2O$ gas at 650 and 750 °C for up to 300 h, forming both protective chromia and regions of Ni-rich oxide. The presence of ash + sulphate mixtures improved Ni–25Cr alloy protection, increasing surface coverage by thin, protective chromia compared with the deposit-free condition. Increasing sulphate proportions in these mixtures led to an accelerated chromia scale growth and reduced internal oxidation zone (IOZ). These beneficial effects were more significant at 750 °C, where surface coverage by the protective scale was increased, and a chromia band was formed beneath nonprotective regions at the IOZ-substrate interface. Alloy additions of Mn and Si generally slowed the growth of outer NiO and IOZ but did not lead to exclusive chromia scale formation.

Keywords Ni-based alloys · Ash · Sulphate · $CO_2 + H_2O$

Introduction

Oxyfuel combustion produces a flue gas rich in CO_2 and H_2O. During combustion, ash particles and alkali sulphate can deposit on the surface of heat-exchangers. Deposit composition varies with boiler configurations (temperature, pressure, etc.), fuel types (low or high sulphur) and so on, and consists mainly of Al_2O_3, SiO_2, Fe_2O_3, CaO and MgO with alkali sulphate [1]. Alkali sulphates can dissolve some

✉ Jianqiang Zhang
  j.q.zhang@unsw.edu.au

  Xuteng Xi
  xuteng.xi@unsw.edu.au

  David J. Young
  d.young@unsw.edu.au

1 School of Materials Science and Engineering, University of New South Wales, Sydney, NSW 2052, Australia

Ⓐ Springer

thermally-grown oxides, thus accelerating corrosion [1]. The ash could serve to retain salts in contact with the metal and contribute to accelerated fireside corrosion [2]. Alternatively, the ash can act as a barrier between gas and metal, slowing the corrosion [1]. Because of the different individual effects of ash and salt on corrosion, it is of interest to determine the effect of deposit sulphate levels on the corrosion behaviour of alloys in a $CO_2 + H_2O$ atmosphere.

Nickel-based alloys are preferred heat-resisting candidates for service at high temperatures, due to their superior corrosion and creep resistance. This paper focuses on the temperature and ash-sulphate effects on corrosion of a Ni–25Cr alloy in a $CO_2 + H_2O$ gas, simulating oxyfuel combustion gas. Alloying with Mn and Si, a common strategy proposed to mitigate alloy corrosion, is also tested in the presence of both ash and salt.

Experimental Procedures

Model alloys Ni–25Cr and Ni–25Cr–2Mn–1Si (all in wt%) were prepared by arc melting pure metals under a protective Ar-5%H_2 gas. The resulting buttons were annealed for homogenization. The resulting Ni–25Cr and Ni–25Cr–2Mn–1Si were fully fcc in structure. Alloys were cut into rectangular shaped coupons, ground to a 1200-grit finish and polished down to 3 μm, followed by electro-polishing. The purpose of electro-polishing was to remove any subsurface deformation zone produced by grinding. As revealed by electropolishing, Ni–25Cr and Ni–25Cr–2Mn–1Si had relatively large grains with elongated shapes, approximately 0.8×2 mm and 0.5×1.5 mm, respectively.

The ash particles were provided by a coal-fired power station, Eraring, with a composition of (SiO_2: 64.6%, Al_2O_3: 24.4%, Fe_2O_3: 2.9%, K_2O: 2.3%, CaO: 1.7%, Na_2O: 0.7%, MgO: 0.6%, with loss on ignition 1.34%, all in wt%). The salts used were Na_2SO_4–K_2SO_4 (50 wt% each). Deposits were prepared by mixing different amounts of ash and sulphates in ethanol then applying the paste to the alloy top surface. The deposits were designed as ash only, ash with 10 wt% salt, ash with 50 wt% salt and ash with 90 wt% salt. The total deposit weight was controlled at 30 ± 5 mg/cm^2. Coated specimens were laid flat on an Al_2O_3 crucible and exposed at 650 and 750 °C to a flowing Ar-60% CO_2–20% H_2O (all vol%) gas with a flowrate of 2 cm/s at reaction temperatures. After 300 h reaction, the samples were cold-mounted in resin and cross-sectioned with an oil-based lubricant. Cross-sections were analysed by optical microscopy, scanning electron microscopy (SEM) and energy dispersive X-ray spectrometry (EDS).

Results

Both protective and non-protective surface areas were observed on Ni–25Cr after 300 h reaction at 650 and 750 °C under the different deposits. The thin protective oxide layer formed at both temperatures was chromia. The fraction of non-protective surface of Ni–25Cr under the deposits was measured by image analysis,

Table 1 Non-protective area (%) on Ni25Cr after 300 h reaction in different conditions

| Condition (°C)	Gas only	Ash only	10 wt% sulphate	50 wt% sulphate	90 wt% sulphate	Sulphate only
650	100	67	75	100	81	95
750	100	59	19	2	95	100
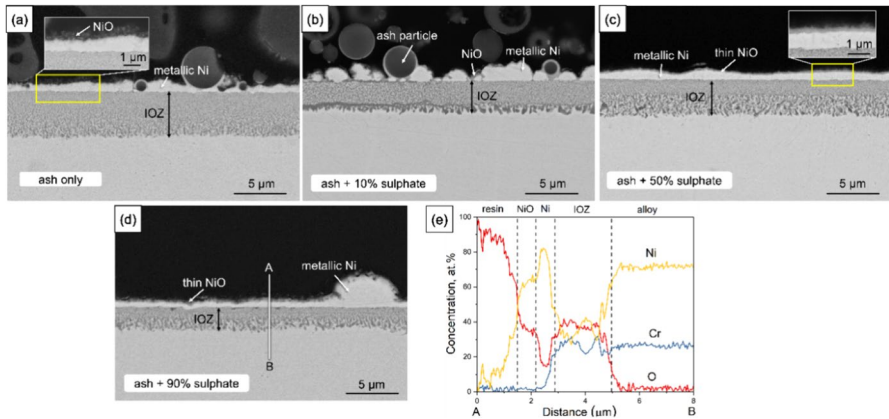
Fig. 1 BSE-SEM cross-sections of multi-layered corrosion products formed on Ni–25Cr after 300 h exposure at 650 °C under deposits of **a** ash only, **b** ash + 10 wt% sulphate, **c** ash + 50 wt% sulphate and **d** ash + 90 wt% sulphate with **e** EDS line scan

yielding the results in Table 1, in which conditions of gas only [3] and sulphate only [4] are also summarized.

The nonprotective corrosion product was multi-layered. Figure 1 shows BSE-SEM images of the non-protective (multi-layered) reaction products on Ni–25Cr under different deposits at 650 °C. Regardless of deposit type, the typical nonprotective reaction products on Ni–25Cr consist of a thick IOZ covered by a metallic Ni layer with a thin NiO on the surface. The IOZ thickness formed under a deposit of ash alone is the largest. A thin NiO layer had grown on the Ni surface and encapsulated some ash particles (Fig. 1a, b). The NiO, Ni and IOZ grown on the alloy were all analysed by EDS. An EDS line scan from the surface toward the alloy (Fig. 1d) under ash + 90 wt% sulphate shown in Fig. 1e differentiates the outer NiO scale, the metallic Ni layer and the Cr enriched IOZ. The fine oxide precipitates in the IOZ were determined by Raman spectroscopy analysis (not shown) to be Cr_2O_3.

Protective scale regions formed on Ni–25Cr had thicknesses below 1 μm for all conditions. Figure 2 shows thin oxide scales formed on the alloy surface under ash only and ash + 10 and 90 wt% sulphate conditions. This thin protective scale was determined to be Cr-rich oxide. Salt residues and NiO particles were found located above the Cr-rich scale (Fig. 2c). A shallow IOZ was found under the thin chromia scale. Particles of Cr-rich sulphide were observed locally beneath the Cr-rich scale

at.%	Ni	Cr	O	S	Na	K	Si
p1	37.9	2.1	52.8	1.9	2.7	2.4	0.3
p2	10.9	30.7	57.9	0.2	-	-	0.4
p3	25.3	40.3	2.5	31.9	-	-	-
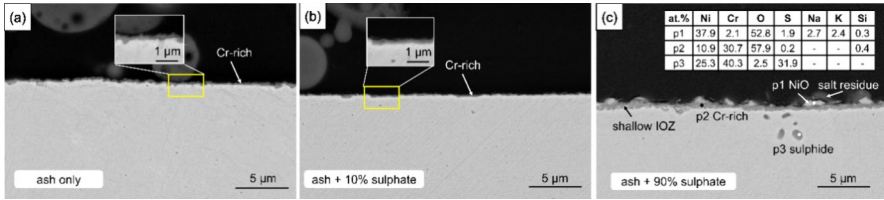
Fig. 2 BSE-SEM cross-sections of thin scale formed on Ni–25Cr after 300 h exposure at 650 °C under deposits of **a** ash only, **b** ash + 10 wt% sulphate and **c** ash + 90 wt% sulphate

under ash + 90 wt% sulphide, but no such sulphides were found after reaction under other deposits.

At 750 °C, both protective and non-protective areas were found on Ni–25Cr alloy under ash + sulphate deposits. Figure 3 shows the BSE-SEM images of nonprotective, multi-layered corrosion products. Under ash alone, an IOZ was formed with a chromia-rich band at the reaction front. Above the IOZ, was a uniform metallic Ni layer covered by a thin outer NiO scale. Under ash + 10 wt% sulphate, the alloy developed the same oxide structure as ash only condition, although the IOZ became thinner with a thicker chromia band. Under ash + 50 wt% sulphate, while most of the surface grew a protective thin scale, localized NiO was formed above a Cr-rich inner scale and no metallic Ni was present. Reaction under ash + 90 wt% sulphate produced a different type of structure: a continuous NiO scale grew on a uniform Ni layer, the IOZ almost disappeared, and a thick Cr-rich band was developed at the reaction front.

An EDS analysis was performed on the corrosion products under ash + 90 wt% sulphate at 750 °C (Fig. 4). An outer NiO scale on a metallic Ni layer are confirmed by elemental maps (Fig. 4c, e). The inner scale was rich in Cr and a Cr-depleted alloy zone is seen immediately beneath it (Fig. 4b). Quantitative EDS point analysis results are listed in Fig. 4f. At the reaction front, chromia intrusions are seen, along with considerable sulphur (around 3.0 at. %).

The protective scales formed on alloy surfaces under different deposits are shown in Fig. 5. They are thin Cr-rich oxide, with a locally uneven scale/alloy interface.

Measured thicknesses of multi-layered reaction products (NiO, Ni, IOZ, Cr_2O_3 band) under different deposits at 650 and 750 °C are shown in Fig. 6. For

Fig. 3 BSE-SEM cross-sections of multi-layered corrosion products formed on Ni–25Cr after 300 h exposure at 750 °C under deposits of **a** ash only, **b** ash + 10 wt% sulphate, **c** ash + 50 wt% sulphate and **d** ash + 90 wt% sulphate
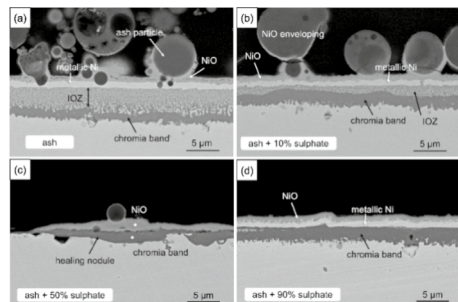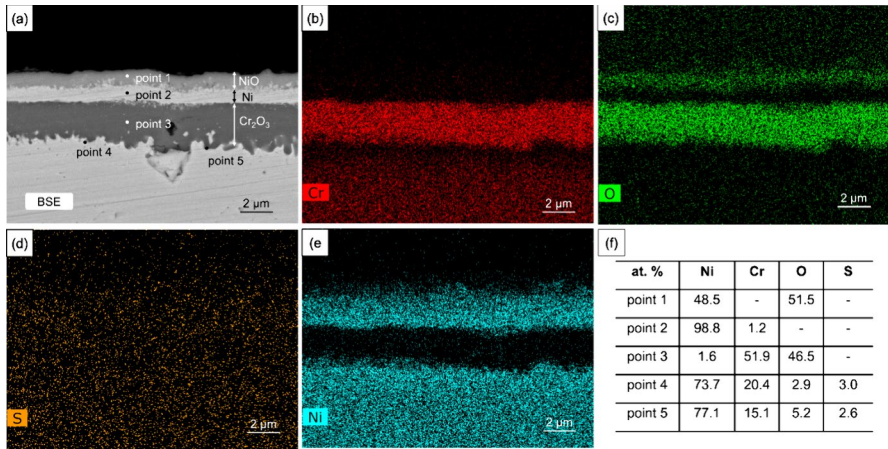
Fig. 4 **a** BSE-SEM cross-section of multi-layered reaction products in Fig. 3d with **b–e** EDS mapping results and **f** EDS point analysis

Fig. 5 BSE-SEM cross-sections of thin scales formed on Ni–25Cr after 300 h exposure at 750 °C under deposits of **a** ash only, **b** ash + 10 wt% sulphate, **c** ash + 50 wt% sulphate and **d** ash + 90 wt% sulphate
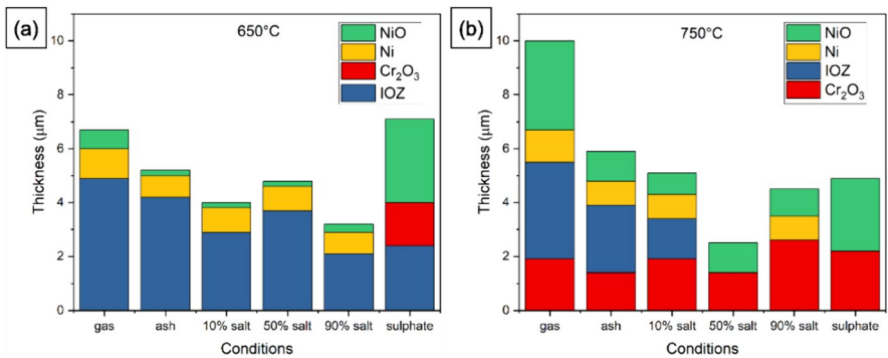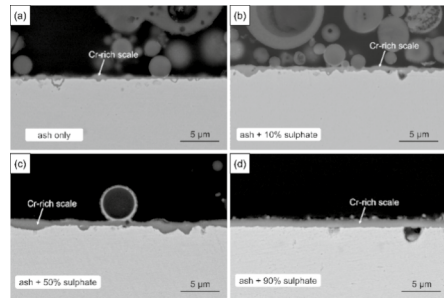
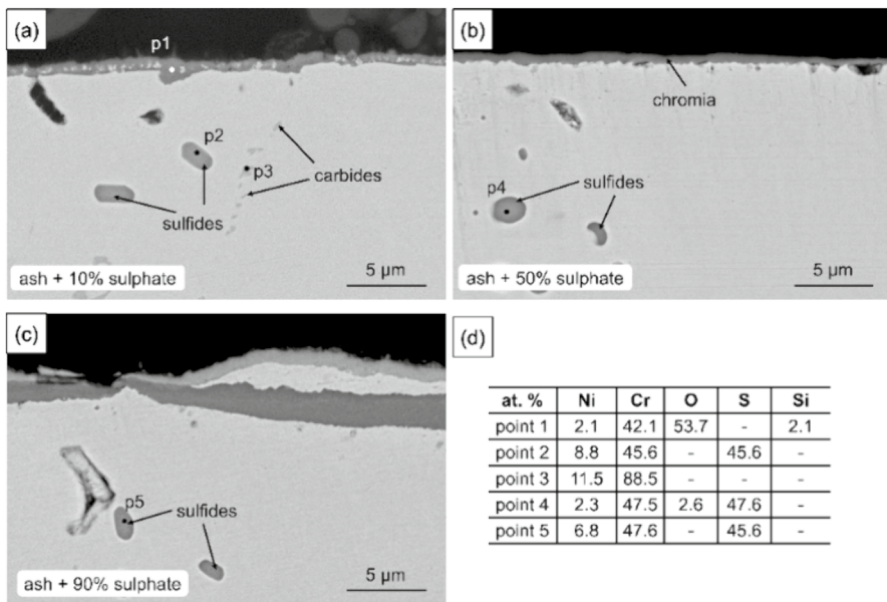
Fig. 6 Thicknesses of multi-layered reaction products formed on Ni − 25Cr under different deposits after 300 h exposure at **a** 650 °C and **b** 750 °C

comparison, results of Ni–25Cr in the gas only and sulphate only conditions are included [3, 4]. At 650 °C, the NiO thickness is the highest in the case of sulphate only (around 3 μm), followed by gas only condition (~0.7 μm). Its growth under other deposits (ash only, ash + 10, 50 and 90 wt% sulphate) is comparatively slow. The Ni layer thickness is slightly higher in the gas only condition (~1.1 μm) than those with ash + sulphate deposits (~0.9 μm). Under sulphate only deposit, the nickel layer was not observed, instead an intermediate chromia band was formed [3]. The gas only, deposit-free condition produced the highest IOZ thickness. Under ash + sulphate mixtures, the IOZ was thinner, especially at 90 wt% sulphate.

At 750 °C, the highest corrosion product thickness was found in the gas only condition. Layers of NiO grown under ash and ash + sulphate deposits are thinner than those with no deposit or with sulphate alone. Ash-containing deposits did not much change Ni metal layer thicknesses, around 0.9 μm under ash, ash + 10 and 90 wt% sulphate compared with 1.2 μm without any deposit. However, no Ni layer was found under ash + 50 wt% sulphate or sulphate only deposits. Although an IOZ was found under ash only and ash + 10 wt% sulphate, it was barely observed when sulphate level was ≥ 50 wt%. Unlike the 650 °C situation, where an internal chromia layer was observed only under a pure sulphate deposit, at 750 °C, Ni–25Cr developed a uniform layer of chromia in all cases. It was thickest under ash + 90 wt% sulphate, and slightly thinner under pure sulphate [4].

Sulphides precipitated at 750 °C inside the alloy under different deposits are shown in Fig. 7. As seen from Fig. 7a, under ash + 10 wt% sulphate, some Cr-rich carbides (EDS point 3) were found along grain-boundaries. Adjacent to the carbides,

at. %	Ni	Cr	O	S	Si
point 1	2.1	42.1	53.7	–	2.1
point 2	8.8	45.6	–	45.6	–
point 3	11.5	88.5	–	–	–
point 4	2.3	47.5	2.6	47.6	–
point 5	6.8	47.6	–	45.6	–

Fig. 7 Sulphides formed in Ni–25Cr under deposits of **a** ash + 10 wt% sulphate, **b** ash + 50 wt% sulphate and **c** ash + 90 wt% sulphate after 300 h exposure at 750 °C with (**d**) EDS point analysis

Cr sulphides were found (EDS point 2). Sulphide precipitation was also observed under an ash + 50 wt% sulphate deposit. Rather multi-layered reaction products were formed under ash + 90 wt% sulphate (Fig. 3). This multi-layered scale tended to be thinner in some areas where Cr-rich sulphides were identified (Fig. 7c).

Alloying elements of Mn and Si did not promote passivation of the alloy surface. As seen in Fig. 8a, their presence did not prevent internal oxidation, extrusion of Ni to the surface or its superficial oxidation. At 750 °C, less metallic Ni was observed: instead, thicker NiO covered the alloy surface (Fig. 8d). The IOZ was also thicker at 750 °C. Manganese was detected in the IOZ, but not in the outer Ni or NiO layer. Silicon was enriched at the reaction front of the IOZ with the alloy matrix (Fig. 8b, c, EDS points 1 and 2), corresponding to a darker image contrast. Increasing sulphate levels in deposits led to thinner NiO layers and internal oxidation zones at 650 and 750 °C. This was most marked under ash + 90 wt% sulphate: a thin NiO layer with metallic Ni grew on top of a shallow IOZ at 650 °C (Fig. 8c), while the IOZ was replaced by a thin Cr-rich band with a continuous silica sublayer at 750 °C (Fig. 8f).

Discussion

When exposed to gas alone, Ni–25Cr underwent breakaway corrosion forming layered structures of $NiO + Ni + IOZ$ at 650 °C [3] and $NiO + Ni + IOZ + Cr_2O_3$ at 750 °C [4]. The presence of ash + sulphate deposits changed alloy protection in a complex way, varying with deposit sulphate content and reaction temperature. The alloy surface was partially protected by a thin Cr-rich scale under deposits of ash alone and ash + sulphate (Fig. 2). In areas where multi-layered corrosion products formed under these deposits, their thicknesses were less than those grown in the gas-only condition at both temperatures (Fig. 6).
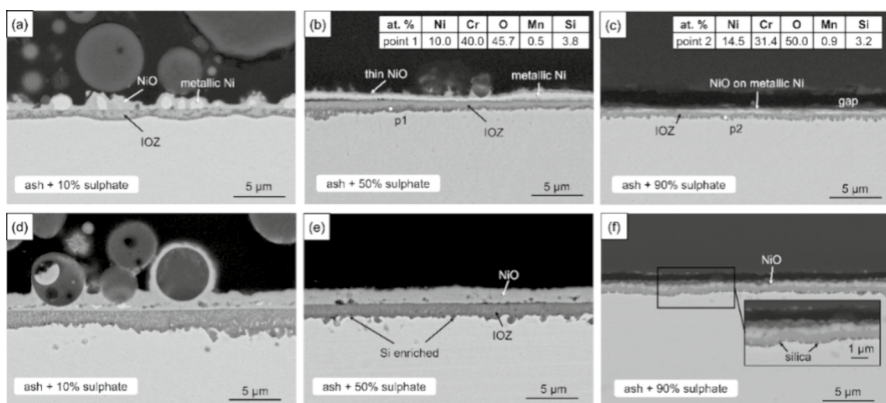
Fig. 8 BSE-SEM cross-sections of multi-layered corrosion products formed on Ni–25Cr–2Mn–1Si after 300 h exposure under deposits of **a** ash + 10 wt% sulphate, **b** ash + 50 wt% sulphate and **c** ash + 90 wt% sulphate at 650 °C and **d** ash + 10 wt% sulphate, **e** ash + 50 wt% sulphate and **f** ash + 90 wt% sulphate at 750 °C

At 650 °C, corrosion under ash alone and ash + 10 wt% sulphate produced partial alloy protection, but further increases in deposit sulphate levels led to reduced protection (Table 1). At 750 °C, adding up to 50 wt% sulphate to the ash was beneficial, increasing the protection up to a maximum of 98% surface coverage under the deposit with 50 wt% sulphate (Table 1). However, increasing sulphate content further to 90 wt% made Ni–25Cr non-protective, forming a predominant structure of NiO + Ni + Cr$_2$O$_3$ (Fig. 3d). The relative thicknesses of multi-layered corrosion products were also affected significantly at 750 °C (Fig. 6). The IOZ was absent under ash + 50 and 90 wt% sulphates (Fig. 3c, d) and a thicker chromia band formed at the reaction front with increasing sulphate level (Fig. 3).

Chromium-rich sulphide formation was found only under ash + 90 wt% sulphate at 650 °C (Fig. 2c), but prevailed at 750 °C under all deposits containing sulphate (Fig. 7). Sulphur was also detected at the chromia band-alloy interface under ash + 90 wt% sulphate deposits at 750 °C (Fig. 4). However, none was found for lower-sulphate deposits. The effect of deposits on the corrosion behaviour of Ni–25Cr alloy, including ash deposit barrier effect and the influence of increasing sulphate levels are now considered.

Effect of Ash Particles

When ash deposits were present, a beneficial effect was observed as a thin chromia scale formed over substantial surface area fractions at both temperatures (Figs. 2 and 5), whereas this protective oxide was absent without ash [3, 4].

Promotion of thin scale formation (α–Al$_2$O$_3$ or Cr$_2$O$_3$) by heterogenous deposits was reported in several studies [5, 6]. The mechanism behind that phenomenon was templating, in which deposit particles promoted iso-structural oxide nucleation, and consequent protective scale growth [5, 6]. In the current study, the industrial ash particles applied to alloy surfaces seemed to have insignificant interaction with underlying chromia scale because the particles (Eraring ash) are mainly amorphous Al, Si-rich oxide. Thus the template effect was not available.

The alloy's ability to form chromia scale is evaluated first. Diffusion theory based on Wagner's model [7] predicts a critical alloy concentration, $N_{Cr}^{(1)}$, required to form an outer chromia scale:

$$N_{Cr}^{(1)} = \left(\frac{\pi g}{2\nu} \frac{V_m}{V_{CrO_\nu}} \frac{N_O^{(S)} D_O}{\tilde{D}_{Cr}} \right)^{\frac{1}{2}} \tag{1}$$

Here g is the critical volume fraction of oxide required to form a continuous layer (often approximated as 0.3 [8]), V_m and V_{CrO_ν} are molar volumes of alloy and oxide, ν the stoichiometric coefficient of CrO$_\nu$, D_O oxygen diffusivity, $\tilde{D}_{Cr}$ Cr interdiffusion coefficient and $N_O^{(S)}$ alloy oxygen solubility. The data used for calculation can be found in refs [4, 9].

Once the chromia scale forms, a sufficient Cr flux from alloy matrix is required to maintain chromia scale growth [10], yielding a second critical Cr concentration ($N_{Cr}^{(2)}$), which is expressed as:

$$N_{Cr}^{(2)} = \frac{V_m}{V_{CrO_v}} \left(\frac{\pi k_p}{2\tilde{D}_{Cr}} \right)^{\frac{1}{2}} \tag{2}$$

where k_p is the parabolic scaling rate constant:

$$X^2 = 2k_p t \tag{3}$$

As no external chromia scale was observed at either 650 or 750 °C in wet CO_2 gas [4, 9], no values of $N_{Cr}^{(2)}$ are available. It is estimated here at 750 °C using chromia scale thicknesses formed on Ni-30Cr in wet CO_2 at 800 °C and in dry CO_2 at 700 °C [9]. For scales grown under ash alone and ash + 90 wt% sulphate, chromia thicknesses were measured from Figs. 2a, c and 5a, d and k_p estimated from Eq. 3. Critical values are summarized in Table 2.

Comparing Cr concentration with two critical values in wet CO_2 gas leads to the prediction that Ni–25Cr ($N_{Cr} = 0.27$) is unable to form chromia scale at 650 °C ($N_{Cr} < N_{Cr}^{(1)}$), while at 750 °C, it could form chromia scale but cannot maintain its growth $\left(N_{Cr}^{(1)} < N_{Cr} < N_{Cr}^{(2)} \right)$. This prediction succeeds for Ni–25Cr without deposits, as no external chromia scale was observed (NiO + Ni + IOZ at 650 °C and NiO + Ni + IOZ + Cr_2O_3 band at 750 °C) [3, 4]. In the presence of ash deposits, along with multi-layered products, Ni–25Cr partially formed a thin chromia scale at both temperatures (Figs. 2 and 5). This observation shows clearly that these deposits facilitated the establishment of chromia scale at 650 °C which is impossible in the gas only condition (Tables 1 and 2).

Chromia scales grown under deposits were maintained up to 300 h reaction. Measured chromia scale thicknesses under ash alone deposits (Figs. 2a and 5a) were 0.29 μm and 0.42 μm at 650 and 750 °C, respectively. Corresponding k_p values were calculated to be 3.8×10^{-16} and $8.2 \times 10^{-16}\,cm^2s^{-1}$ at 650 and 750 °C. It is seen that the chromia scale growth rate was reduced significantly (Table 2) in the presence of ash deposits. Similarly, the multi-layered scales formed under ash + sulphate had lower thicknesses than those grown in gas alone (Fig. 6). All observations indicate

Table 2 Critical Cr alloy levels for external chromia scale formation and growth on Ni–Cr alloys

T (°C)	$N_{Cr}^{(1)}$	$N_{Cr}^{(2)}$			$k_p(10^{-16}cm^2s^{-1})$		
		wet CO_2	Under ash	Under ash + 90% sulphate	wet CO_2	Under ash	Under ash + 90% sulphate
650	0.31	N/A	0.22	0.31	N/A	3.8	7.2
750	0.22	0.27–0.39	0.06	0.15	63–490	8.2	54.5

a reduction in p_{O_2} beneath the deposit. On this basis it is concluded that the ash deposit acts as a partial barrier to gas transport. Rapid consumption of oxygen by reaction with the alloy beneath the deposit results in an oxygen activity gradient developing across the deposit layer. This process continues until a steady-state is reached, with a low p_{O_2} at the deposit-oxide interface.

Chromia has complex semi-conduction properties. It was reported that a double layered chromia scale formed on pure Cr with the inner part n-type and outer part of p-type [11]. If p-type behaviour prevails in the current study, the parabolic growth rate constant for chromia scale growth is expressed as [12]

$$k_p = \int_{a_{O_2}^1}^{a_{O_2}^2} D_{eff} d(ln a_{O_2})$$

(4)

Here $a_{O_2}^1$ and $a_{O_2}^2$ are the oxygen activities at the oxide/alloy and oxide/gas interface, respectively; D_{eff} is the effective diffusion coefficient. The $a_{O_2}^1$ value is set by the chromia-alloy interface equilibrium, i.e. Cr_2O_3 dissociation partial pressure. At the scale/gas interface, beneath an ash deposit, the value of $a_{O_2}^2$ is lower than in the gas, leading to a reduced k_p. This qualitatively explains the improved alloy ability to maintain chromia scale growth on Ni–25Cr (Table 2), the experimentally observed result (Figs. 2a and 5a).

Effect of Sulphate

Protective chromia scale regions formed under ash + sulphate mixtures were thicker at higher sulphate levels, an effect more marked at 750 °C (Figs. 2 and 5). For non-protective regions, the IOZ thickness was reduced with higher levels of sulphate in the deposit at 650 °C. This effect is more significant at 750 °C (Fig. 6). Increasing sulphate level in deposits reduced the fraction of protected Ni–25Cr surface at 650 °C, but at 750 °C promoted the surface protection for sulphate levels ≤ 50 wt%. However, further increases in sulphate level reduced the extent of passivation (Table 1).

The sulphate salt deposited on the alloy surface can release S-containing species by the reaction:

$$(Na, K)_2SO_4 = (Na, K)_2O \text{ (in sulphate)} + SO_3(g)$$

(5)

in which $(Na, K)_2O$ remains in the sulphate, and SO_3 can further dissociate according to:

$$SO_3(g) = SO_2(g) + \frac{1}{2}O_2(g)$$

(6)

$$SO_2(g) = \frac{1}{2}S_2(g) + O_2(g)$$

(7)
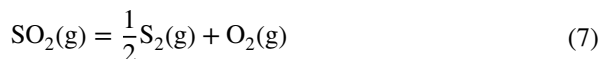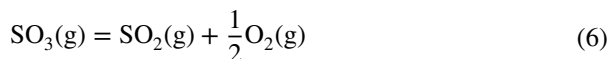
Table 3 Gas minority species pressures (atm) produced by ash + sulphate deposits in equilibrium with Ar–60CO$_2$–20H$_2$O

Temperature (°C)	O$_2$	SO$_2$	SO$_3$	Na$_2$SO$_4$	K$_2$SO$_4$
650	1.5E−8	2.3E−9	1.4E−12	1.1 E−11	4.1 E−11
750	1.7E−7	6.8E−8	3.9 E−11	6.5 E−10	2.4 E−9

The minority gas species of ash + sulphate deposits in equilibrium with Ar–60CO$_2$–20H$_2$O are calculated by FactSage and shown in Table 3, assuming the ash to be chemically inert. Beneath ash-bearing deposits, however, the value of p_{O_2} is lowered, as shown in the previous section. Given that p_{SO_3} is fixed by salt dissociation, this results in increased values of p_{SO_2} and p_{S_2} in contact with the alloy or its corrosion products.

The minimum value of p_{O_2} beneath the deposit, due to salt decomposition alone, is still enough to stabilise NiO, and reasons for alterations in chromia scaling must be sought elsewhere. In view of the increased sulphur activity beneath salt deposits, its consequences are examined. Segregation of S species on chromia grain-boundaries leads to much finer grains [13], and therefore accelerated scale growth. Faster chromia nucleation and growth leads to a greater extent of alloy surface protection, provided that the alloy can maintain exclusive chromia growth [14, 15]. To investigate further, the $N_{Cr}^{(2)}$ value under ash + 90 wt% sulphate is calculated (Table 2).

Chromia scale thicknesses under ash + 90 wt% sulphate were 0.39 μm at 650 °C and 1.09 μm at 750 °C, compared with ash alone cases (0.29 and 0.42 μm respectively). The higher growth rate of chromia under ash + 90 wt% sulphate (Table 2) is consistent with our previous finding [15] that Cr$_2$O$_3$ growth was accelerated in an SO$_2$-containing environment. At 650 °C, the fast chromia growth under ash + 90 wt% sulphate increased $N_{Cr}^{(2)}$ to 0.31. Clearly, Ni–25Cr cannot maintain such fast chromia growth: as seen from Fig. 2c, small regions of external NiO and internal oxidation had formed near a thin chromia scale.

At 750 °C, $N_{Cr}^{(2)} = 0.15$, as calculated using the k_p under ash + 90 wt% sulphate, a value less than the N$_{Cr}$ of alloy. Thus the accelerated growth of chromia by sulphate-bearing deposit can be compensated by the fast supply of Cr for Ni–25Cr at 750 C, but not at 650 °C.

For non-protective regions, the IOZ thickness was reduced with higher levels of sulphate in the deposit at 650 °C. This effect is more significant at 750 °C (Fig. 6). For the deposit sulphate levels > 10 wt% at 750 °C, IOZ growth was stopped by formation of a chromia band at the scale/alloy interface. The reduced IOZ thickness is thereby explained.

It is seen from Table 1 that both ash and sulphate affected the fraction of protected surface area by Cr$_2$O$_3$ formation. Results at 650 °C are not self-consistent, possibly due to non-uniformity of the applied deposits. Attention is therefore focused on results at 750 °C, where a maximum in protection appeared at 50 wt% sulphate. Ash particles had a barrier effect, promoting chromia formation. As argued above, addition of sulphate to ash deposits accelerated chromia growth, leading to the observed increase in surface area coverage by protective scale.

In contrast, pure sulphate did not lead to thin chromia scale formation, but did form a somewhat protective duplex scale of outer NiO and inner chromia layers (plus internal sulphides) at 750 °C [4]. The interplay between ash and sulphate effects under mixed deposits at high sulphate levels is not yet understood.

As for the sulphide formation, the low p_{O_2} at chromia-alloy interface led to elevated p_{S_2} which facilitates sulphide formation. The Cr-sulphide was only observed beneath chromia scale, but not under multi-layered NiO + Ni + IOZ products where the Ni/NiO equilibrium controls p_{O_2} at a high value, and p_{S_2} is too low for internal sulphide formation.

Effect of Mn + Si

The addition of Mn and Si to Ni–25Cr led to microstructurally similar, non-protective corrosion. Outer NiO layer and IOZ growth were slower, but protective chromia scale did not develop anywhere on the surface. Manganese was present in the IOZ, but not in the Ni or NiO layers. Silicon was enriched at the IOZ reaction front (Fig. 8). The well-known beneficial effects of Mn and Si in slowing mass transport during corrosion are evident, but the failure of the doped alloy to at least partially passivate during under-deposit corrosion is not yet understood.

Conclusion

Under gas-only conditions, Ni–25Cr experienced breakaway oxidation at both 650 and 750 °C. When ash deposits were present on the alloy surface, a beneficial effect of this deposit was observed, as an increased surface area covered by protective Cr-rich scales was observed at both temperatures. This effect is attributed to the barrier effect of these deposits in lowering the oxygen activity and promoting chromia scale formation.

Increasing sulphate levels in deposits accelerated the growth of chromia scale at both temperatures by refining the oxide grains. At 650 °C, a detrimental effect of this acceleration was observed as alloy Cr diffusion cannot maintain the accelerated scale growth. At 750 °C, chromia growth is maintained by faster alloy Cr diffusion. For non-protective regions, the IOZ thickness was reduced at higher level of sulphate, due to the acceleration by S of continuous chromia layer growth at the IOZ-alloy interface. Both ash and sulphate affected the fraction of protected surface area. At 750 °C protection of Ni–25Cr was increased with higher sulphate deposit levels up to 50 wt%, due to acceleration by S of chromia growth. However, Ni–25Cr was predominantly non-protective at deposit sulphate levels ≥ 90 wt%.

The addition of Mn and Si in Ni–25Cr generally slowed down the mass transport during corrosion but did not lead to any passivation under these deposits.

These results provide important insights into the under-deposit corrosion behaviour of chromia-forming Ni-based alloys in the oxyfuel combustion process.

Data Availability The raw/processed data required to reproduce these findings cannot be shared at this time as the data also forms part of an ongoing study.

Declarations

Conflict of interest The authors declare no competing interests.

References

1. G. H. Meier, *Oxidation of Metals* **98**, (1), 2022 (1).
2. T. Furugaki, H. Takahashi, and S. Hayashi, *Oxidation of Metals* **98**, 2022 (511).
3. Y. Cai, X. Xi, J. Zhang, B. Gleeson, and D. J. Young, *Materials at High Temperatures* **40**, 2023 (260).
4. Y. Xie, Y. Cai, J. Zhang, B. Gleeson, and D. J. Young, *Corrosion Science* **181**, 2021 109227.
5. Y. Kitajima, S. Hayashi, T. Nishimoto, T. Narita, and S. Ukai, *Oxidation of Metals* **73**, (3), 2010 (375).
6. Y. Xie, Y. Huang, Y. Li, and X. Peng, *Corrosion Science* **190**, 2021 109717.
7. C. Wagner, *Zeit Elektrochem* **63**, 1959 (772).
8. R. A. Rapp, *Acta Metallurgica* **9**, 1961 (730).
9. Y. Xie, J. Zhang, and D. J. Young, *Journal of the Electrochemical Society* **164**, 2017 (C285).
10. C. Wagner, *Journal of the Electrochemical Society* **99**, 1952 (369).
11. L. Latu-Romain, Y. Parsa, S. Mathieu, M. Vilasi, and Y. Wouters, *Oxidation of Metals* **90**, 2018 (255).
12. A. Atkinson, *Reviews of Modern Physics* **57**, 1985 (437).
13. C. Sha, L. Yang, J. M. Cairney, J. Zhang, and D. J. Young, *Corrosion Science* **222**, 2023 111410.
14. G. Luckman and R. S. Polizzotti, *Metallurgical Transactions A* **16**, 1985 (133).
15. C. Yu, T. D. Nguyen, J. Zhang, and D. J. Young, *Journal of the Electrochemical Society* **163**, 2016 (C106).

Publisher's Note Springer Nature remains neutral with regard to jurisdictional claims in published maps and institutional affiliations.